



This is a repository copy of *Brainstem neuroadaptations in rodent models of Parkinson's disease*.

White Rose Research Online URL for this paper:

<https://eprints.whiterose.ac.uk/225036/>

Version: Published Version

Article:

Al Tannir, R., Pautrat, A., Soutrenon, R. et al. (2 more authors) (2025) Brainstem neuroadaptations in rodent models of Parkinson's disease. *European Journal of Neuroscience*, 61 (7). e70068. ISSN 0953-816X

<https://doi.org/10.1111/ejn.70068>

© 2025 The Author(s). *European Journal of Neuroscience* published by Federation of European Neuroscience Societies and John Wiley & Sons Ltd. This is an open access article under the terms of the Creative Commons Attribution-NonCommercial-NoDerivs License (<http://creativecommons.org/licenses/by-nc-nd/4.0/>), which permits use and distribution in any medium, provided the original work is properly cited, the use is non-commercial and no modifications or adaptations are made.

Reuse

This article is distributed under the terms of the Creative Commons Attribution-NonCommercial-NoDerivs (CC BY-NC-ND) licence. This licence only allows you to download this work and share it with others as long as you credit the authors, but you can't change the article in any way or use it commercially. More information and the full terms of the licence here: <https://creativecommons.org/licenses/>

Takedown

If you consider content in White Rose Research Online to be in breach of UK law, please notify us by emailing eprints@whiterose.ac.uk including the URL of the record and the reason for the withdrawal request.



eprints@whiterose.ac.uk
<https://eprints.whiterose.ac.uk/>

SPECIAL ISSUE ARTICLE **OPEN ACCESS**

Basal Ganglia and Related Disorders: From Cellular and Circuit Dysfunctions to Therapy

Brainstem Neuroadaptations in Rodent Models of Parkinson's Disease

Racha Al Tannir¹ | Arnaud Pautrat¹ | Remi Soutrenon¹ | Paul G. Overton² | Veronique Coizet¹ ¹Université Grenoble Alpes, Inserm U1216, CHU Grenoble Alpes, Grenoble Institut Neurosciences, Grenoble, France | ²Department of Psychology, University of Sheffield, Sheffield, UK**Correspondence:** Veronique Coizet (veronique.coizet@univ-grenoble-alpes.fr)**Received:** 24 May 2024 | **Revised:** 11 January 2025 | **Accepted:** 22 January 2025**Associate Editor:** Yoland Smith**Funding:** This work was funded by the Institut National de la Santé et de la Recherche Médicale (Inserm) and the Network of Centres of Excellence in Neurodegeneration (CoEN) and supported by the École doctorale Chimie et sciences du vivant, Université Grenoble Alpes.**Keywords:** dendritic spines | GABA_A receptors | Parkinson's disease | periaqueductal gray | superior colliculus

ABSTRACT

A classical theory of a key pathophysiological change in Parkinson's disease (PD) is that GABAergic neurons in the substantia nigra pars reticulata (SNr), an output structure of the basal ganglia, become hyperactive following the dopaminergic loss. Increased GABA release from the SNr neurons is thus likely to induce neuroadaptations in structures receiving a direct projection from the SNr, including the parabrachial nucleus (PBN), superior colliculus (SC), and periaqueductal gray (PAG). We have shown that the PBN indeed exhibits cellular and molecular changes in PD rat models. We thus expected the SC and the PAG to likewise show neuroplasticity. The objective of the present work was to evaluate the cellular and molecular plasticity in both the SC (lateral and medial) and the PAG in PD rats with a partial or total dopaminergic lesion. We used Golgi–Cox to measure the spine density and spine morphology and Western blot to analyze GABA_A receptor expression in both PD rat models compared to sham animals. We found an increase in spine density (thin and stubby types) following total dopaminergic lesions in the SC and the PAG. Additionally, increased GABA_A receptor expression was observed in the lateral SC in the total lesion group only. These results suggest compensatory mechanisms in PD that may delay disease onset and contribute to both motor and nonmotor symptoms. Further investigation should be performed to fully understand the functional impact of the plasticity revealed in this work.

1 | Introduction

Parkinson's disease (PD) is characterized by a progressive degeneration of dopaminergic (DA) neurons located in the substantia nigra pars compacta (SNc). This neuronal loss disrupts the function of the basal ganglia, a highly organized network crucial for goal-directed behavior and action selection (Mink 1996; Redgrave

et al. 1999, 2010). A classical theory regarding PD pathophysiology states that GABAergic neurons from the substantia nigra pars reticulata (SNr), a main output structure of the basal ganglia (Albin et al. 1989), become hyperactive following the loss of dopamine (Bergman et al. 1994; Hassani et al. 1996). This hyperactivity suggests that there is an intensified inhibitory influence of the SNr on its targets. Notably, the main structures receiving direct

Abbreviations: 6-OHDA, 6-hydroxydopamine; AP, anteroposterior; BSA, bovine serum albumin; DA, dopaminergic; DAB, 3,3'-diaminobenzidine; DV, dorsoventral; IOD, integrated optical density; ML, mediolateral; NHS, normal horse serum; OD, optical density; PAG, periaqueductal gray; PB, phosphate buffer; PBN, parabrachial nucleus; PD, Parkinson's disease; SC, superior colliculus; SDS, sodium dodecyl sulfate; SNc, substantia nigra pars compacta; SNr, substantia nigra pars reticulata; TH, tyrosine hydroxylase; TX, Triton X-100.

This is an open access article under the terms of the [Creative Commons Attribution-NonCommercial-NoDerivs](https://creativecommons.org/licenses/by-nc-nd/4.0/) License, which permits use and distribution in any medium, provided the original work is properly cited, the use is non-commercial and no modifications or adaptations are made.

© 2025 The Author(s). *European Journal of Neuroscience* published by Federation of European Neuroscience Societies and John Wiley & Sons Ltd.

projections from the SNr are the thalamus such as the ventromedial thalamic nucleus (Carpenter 1976; Clavier et al. 1976) and numerous structures in the brainstem, including the pedunclopontine tegmental nucleus, the superior colliculus (SC), the parabrachial nucleus (PBN), and the periaqueductal gray (PAG) (Deniau and Chevalier 1992; Hopkins and Niessen 1976; Schneider 1986; Spann and Grofova 1991). Although the thalamus and pedunclopontine tegmental nucleus have received considerable attention in PD research (Blesa et al. 2016; Pahapill and Lozano 2000; Tubert et al. 2019; Villalba et al. 2014), the functional status of the SC, PBN, and PAG in PD remains relatively unexplored despite their close connectivity with the basal ganglia and the suggested pathological link between the SNr and these structures. We have previously demonstrated that the SC exhibits abnormal hypersensitivity to visual stimuli in PD rat models and de novo PD patients (Moro et al. 2020; Rolland et al. 2013). Additionally, we found diminished nociceptive responses in the PBN following a total DA lesion in the SNc (Pautrat et al. 2023). Our previous work also provided indirect electrophysiological evidence suggesting that increased inhibitory input from the SNr in PD induces neuroplasticity changes in the SC and PBN (Pautrat et al. 2023; Rolland et al. 2013). On the basis of this evidence, we further investigated the anatomical, cellular, and molecular basis for neuroplasticity in the PBN. Our findings revealed an increase in the density of dendritic spines, suggested their turnover is increased, and showed decreased postsynaptic densities following partial or total DA lesions in the SNc. Furthermore, we found a significant increase in GABA_A receptor expression in the PBN following a total DA lesion, but not a partial DA lesion (Pautrat et al. 2023).

Compensatory mechanisms in PD have been suggested to delay the clinical onset of the disease but also to play a role in the development of motor and nonmotor symptoms (Blesa et al. 2017). Molecular and cellular compensatory mechanisms have mainly been studied within the basal ganglia (Arkadir et al. 2014; Bezard and Gross 1998; Blesa et al. 2017), but our findings suggest that important changes can also take place at the level of their targets. These changes are likely to play a significant role in the pathological changes underlying PD as the disorder progresses. Having previously reported compensatory neuroadaptations in the PBN (Pautrat et al. 2023), our main objective in this study was to evaluate the cellular (using Golgi–Cox for spine density and morphology) and molecular (via Western blot for GABA_A receptor expression) bases for neuroadaptive plasticity in both the SC and PAG in hemiparkinsonian rats with either a partial or total DA denervation in the SNc (Pautrat et al. 2023). Our hypothesis was that the SC and the PAG would show similar cellular and molecular changes to those described in the PBN because these structures also receive a direct projection from the SNr. The nigroreticular pathway heavily projects to the lateral part of the SC and to a lesser extent to the medial regions of this structure (Harting et al. 1988), and hence, we performed a separate analysis on the medial and lateral SCs.

2 | Methods

2.1 | Animals

Male Long–Evans rats were used for these experiments. They were kept in standard environmental conditions (12-h light/dark cycle) at a constant temperature of 22°C, with food and water

provided ad libitum. The experiments were carried out in accordance with the policy of Lyon 1 University, the Grenoble Institut des Neurosciences (GIN), and French legislation. Experiments were conducted in compliance with the European Community Council Directive of November 24, 1986 (86/609/EEC). The research was authorized by the Direction Department of Veterinary Services of Isère—Ministry of Agriculture and Fisheries, France (Coizet, Véronique, PhD, Permit Number 381003). Every effort was made to minimize the number of animals used and their suffering during the experimental procedures. All procedures were reviewed and validated by the “Comité éthique du GIN n°004” agreed upon by the research ministry.

2.2 | 6-Hydroxydopamine (6-OHDA) Lesions

Male Long–Evans rats ($n=63$) were anesthetized with isoflurane gas and placed in a stereotaxic frame. Their heads were shaved, cleaned, and disinfected with Vétédine. Animals were given a subcutaneous injection of a local anesthetic (lidocaine) before a midline incision was performed and the scalp retracted to allow access to the skull. A burr hole was then drilled above the SNc on the right-hand side of the midline, and the toxin 6-OHDA (Sigma-Aldrich, USA, 2.6 mg/mL) was injected with a 30G cannula connected with polyethylene tubing to a 10- μ L Hamilton syringe, driven by an infusion pump at 0.5 μ L/min. At the end of the injection, the cannula was kept in place for 5 min to allow the toxin to diffuse. Three animal groups were prepared:

- i. Partial DA lesion animals (partial DA lesion, $n=14$) received 1.0 μ L of 6-OHDA at the following coordinates: anteroposterior (AP): +3.0 mm; mediolateral (ML): +2.4 mm; and dorsoventral (DV): +2.4 mm from interaural zero.
- ii. Total DA lesion animals (total DA lesion, $n=25$) received 3.0 μ L of 6-OHDA at the following coordinates: AP: +3.0 mm; ML: +2.1 mm; and DV: +2.5 mm from interaural zero.
- iii. Control animals received vehicle (sterile 0.9% NaCl) without the toxin (sham, $n=24$) at the following coordinates: AP: +3.0 mm; ML: +2.4 mm; and DV: +2.4 mm from interaural zero.

These coordinates were calculated according to the rat brain atlas of Paxinos and Watson (2007). The DA degeneration occurs during the first 2 weeks' postinjection of the toxin, before reaching a baseline during the third week.

2.3 | Golgi Staining

Three weeks after the 6-OHDA lesion, rats ($n=3$ in each experimental group) were euthanized with an overdose of pentobarbital (150 mg/kg, ip) and perfused with 250 mL of 0.9% saline followed by 250 mL of 4% formaldehyde. The brains were collected and placed in 4% formaldehyde overnight for postfixation and then placed in Golgi–Cox solution (1% potassium dichromate, 1% potassium chromate, and 1% mercuric chloride) for 2 days. The solution was then replaced by a fresh one, and the brains were immersed for 12 more days.

The incubation (total of 14 days) was done in the dark at room temperature. Afterwards, the brains were washed in 1% potassium dichromate for 24 h, placed in 20% sucrose for 24 h for cryo-protection, and then snap-frozen in -60°C isopentane. Two series of sagittal brain sections were cut. The first one consisted of $30\text{-}\mu\text{m}$ -thick slices centered on the SNc (AP: $-5.2/-5.8$ mm behind bregma) and was collected in antifreeze solution and stored at -20°C for anti-tyrosine hydroxylase (TH) immunohistochemistry. The second one consisted in $80\text{-}\mu\text{m}$ -thick slices centered on the SC and PAG collected directly onto gelatin-coated slides. This thickness and sagittal orientation allowed optimal preservation of the tissue and observation of spines on the secondary and tertiary dendritic segments. Indeed, unlike the PBN (Pautrat et al. 2023), it was not possible to identify a dendrite with sufficient length and observe sufficient dendritic spines when using coronal sections. Microscope slides were then developed with Kodak rapid fix diluted at 1:6 in distilled water, dehydrated in alcohols, and coverslipped in DPX. Slides were allowed to dry at room temperature for 72 h, after which they were cleaned and scanned.

2.4 | Golgi Reconstruct

Slides stained with the Golgi–Cox technique were scanned using Zeiss Axio Scan.Z1 (Zeiss, Germany) at $40\times$ magnification. Ten Z stacks with a $2.0\text{-}\mu\text{m}$ step were taken, centered on either the entire SC or PAG region. Images were imported into RECONSTRUCT software that utilizes the distinct geometric characteristics of spines for their categorization (Fiala 2005; Risher et al. 2014). Dendritic sections of neurons clearly located in the deep lateral and medial SC and in the lateral/ventrolateral PAG were analyzed. With the RECONSTRUCT software, the experimenter identified each dendritic segment to analyze by drawing a line along the dendrite (which in every case was clearly connected to a cell body, Figure 1A) as well as along the shafts of the associated dendritic spines and across the width of the spine heads. The software then extracted measurements based on the selected dendrites and spines. Parameters such as spine length, width, and number were then measured. The software classifies spine morphology automatically based on these measurements, providing information such as dendrite length, width, total spine count, percentage of mushroom/stubby/filopodial/branched/long thin/thin spines, and spine density. This approach utilizes the distinct geometric characteristics of spines as the basis for their categorization (see Figure 1B, Risher et al. 2014):

- Filopodial: length $> 2\text{ }\mu\text{m}$
- Long thin: length > 1 and $\leq 2\text{ }\mu\text{m}$
- Thin: length $\leq 1\text{ }\mu\text{m}$
- Stubby: length/width ratio < 1
- Mushroom: width $> 0.6\text{ }\mu\text{m}$
- Branched: two heads or more

According to Risher et al. (2014), with this method, users can expect to spend considerably less time and conduct an unbiased classification of spines. Quantification achieved with this

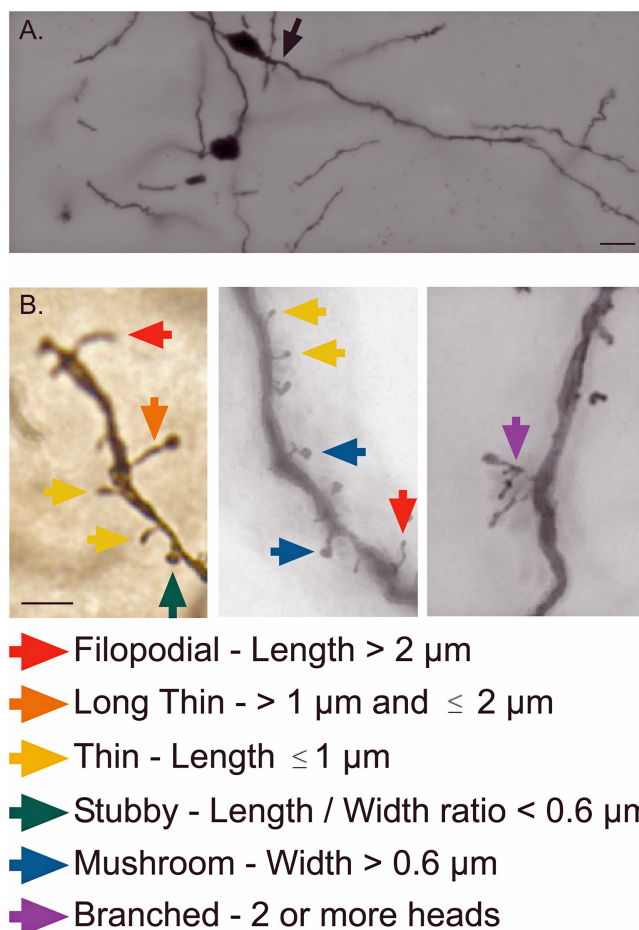


FIGURE 1 | Golgi–Cox analysis: (A) Photomicrographs illustrating the identification of dendritic spines clearly connected to a cell body (black arrow). Scale bar: $10\text{ }\mu\text{m}$. (B) Top panel: photomicrographs of dendritic spines labeled with Golgi–Cox staining illustrating the different types of spines analyzed: filopodial (red), long thin (orange), thin (yellow), stubby (green), mushroom (blue), and branched (purple). Bottom panel: criteria used in the present study according to Risher et al. (2014) to classify the different spine types. Scale bar: $2\text{ }\mu\text{m}$.

method can also be reliably compared to data obtained from other users, providing some much needed consistency to the analysis of spines.

We analyzed the dendritic spines density and spine morphology as follows:

- $n \geq 5$ dendrites per animal (each from a different neuron)
- Total length of dendritic segments analyzed per animal: $600\text{ }\mu\text{m}$
- Three animals per experimental group
- Total dendritic length analyzed per group: $\sim 1800\text{ }\mu\text{m}$ ($\sim 600 \times 3$)

The number of dendrites was used as the sample size for statistical analysis.

In addition to the current Golgi experiments conducted in the SC and PAG, we analyzed Golgi data from the PBN obtained in

a previous study (Pautrat et al. 2023). The experimental groups, the number of rats per group ($N=3$), and the methodology for Golgi staining were identical to those used in the present study.

2.5 | Western Blot

This analysis included a total of 30 rats for the lateral SC (sham: $n=9$; partial DA group: $n=8$; and total DA group: $n=13$), 45 rats for the medial SC (sham: $n=17$; partial DA group: $n=11$; and total DA group: $n=17$), and 27 rats for the PAG (sham: $n=7$; partial DA group: $n=9$; and total DA group: $n=11$). Three weeks after the 6-OHDA lesion, animals were deeply anesthetized using isoflurane before immediate decapitation and brain sampling. The brains were quickly frozen in isopentyl (-60°C), and two series of coronal brain sections were cut in a cryostat. The first consisted of 30- μm slices centered on the SNc (AP: $-5.2/-5.8$ mm behind bregma) collected on slides for anti-TH immunohistochemistry. The second one consisted of 80- μm -thick slices centered on the entire AP length of the SC and PAG. The lateral SC, medial SC, and PAG were then isolated using a tissue punch, and all samples were stored at -80° until Western blot processing. The samples were then homogenized in a cold 10% sodium dodecyl sulfate (SDS) solution with a protease inhibitor cocktail tablet (Sigma-Aldrich, USA). The homogenized solution was centrifuged at $15,000\times g$ for 15 min at 4°C , and the clear supernatant was collected. Following a BCA protein assay, the samples were diluted and mixed with $4\times$ SDS sample buffer (Laemmli with beta-mercaptoethanol, Bio-Rad Laboratories, USA), boiled at 95°C for 10 min, cooled, and then centrifuged at $10,000\times g$ for 2 min. Equal amounts of protein (20 μg) for each group were resolved using 10% SDS-PAGE. Proteins were then electrophoretically transferred to a PVDF membrane (GE Healthcare, Germany) for 1 h 15 min. The transferred proteins were then blocked with 3% bovine serum albumin (BSA) in TBS-T for 2 h at room temperature. The blot was then incubated overnight at 4°C with the following primary antibodies: rabbit anti-GABA_A R $\alpha 1$ (1:2000, Sigma-Aldrich, Germany) and rabbit anti-GAPDH (1:2000, Sigma-Aldrich, USA). After incubation, the blots were washed with TBS-T three times for 10 min each. The blots were incubated with antirabbit horseradish peroxidase-conjugated secondary antibody (1:10,000, Cell Signaling, USA) for 2 h. After washing three times (each wash for 10 min), ECL Plus Substrate (Thermo Fisher, USA) was applied to the blots for 5 min in the dark. The blots were revealed using the ChemiDoc Imaging System (Bio-Rad Laboratories, USA), and the protein expression intensity was assessed by integrated optical density (IOD). To account for possible differences in total protein load, the results of the measurements were presented as a ratio of IOD of GABA_A receptor protein to the IOD of the respective GAPDH using ImageJ software (Bio-Rad Laboratories, USA).

2.6 | Histology 6-OHDA Lesions

The extent of the DA denervation induced by 6-OHDA injections in the SNc was determined in all animals from this experiment using TH immunohistochemistry on free-floating slices (Golgi-Cox material) or directly on slides (Western blot material). To reveal TH, the sections were washed and incubated in a blocking solution containing 0.1-M phosphate buffer (PB) with 0.3% of

Triton X-100 (TX), 2.5% BSA, and 5% normal horse serum (NHS) for 2 h before being transferred overnight to a 0.1-M PB-TX 0.3% with 1% BSA and 2% NHS containing the primary mouse monoclonal TH antibody, diluted 1:3000 (Chemicon, UK). The following day, sections were washed in 0.1-M PB and incubated with the secondary antibody, biotinylated antimouse made in horse (in a dilution of 1:1000 in 0.1-M PB-TX 0.3% with 2% NHS) for 2 h. Following further washes in 0.1-M PB, the sections were exposed to the elite VECTASTAIN ABC reagent (Vector Laboratories, USA) diluted 1:100 in PB-TX 0.3% for 2 h. Again, following washes in 0.1-M PB, immunoreactivity was revealed by exposure to nickel-enhanced 3,3'-diaminobenzidine (DAB, Sigma-Aldrich, USA) for 2 min, which produced a black reaction product. Sections were then mounted onto gelatin-coated slides, dehydrated through alcohols, and cleared in xylene before being coverslipped with DPX. TH immunolabeling of DA neurons in the SNc (-6.00 to -6.30 mm AP relative to bregma, one section per rat) was evaluated using a light microscope (Nikon Eclipse 80i, TRIBVN, France) coupled to the ICS Framework computerized image analysis system (TRIBVN, Version 2.9.2, France). For quantification, TH-labeled sections of the SNc were digitized using a Pike F-421C camera (Allied Vision Technologies, Germany). Optical densities (ODs) were then measured in all animals from this experiment for the denervated hemisphere (right) and nondenervated hemisphere (left) of operated animals. OD of the lesioned hemisphere was then compared to the nonlesioned hemisphere in each animal.

In all animals from this experiment, we used a Stereo Investigator software (Stereo Investigator 2022.3.1, MBF Bioscience LLC, Williston, VT, USA) to manually count TH cells in the SNc. The SNc was delineated with a $2\times$ objective (Olympus, BX53) at the level of -6.00 to -6.30 mm AP relative to bregma (one section per rat). Cell counting was performed using a $40\times$ objective throughout the SNc, with a 100% sampling grid and a 60×60 - μm counting frame.

2.7 | Statistics

All statistical tests were performed using GraphPad Prism Version 6.01 (Dotmatics, USA) software. The Shapiro-Wilk test was used to assess the normality of the different data distributions. The statistical reliability of differences between the three groups for all data was assessed using ANOVA followed by a Tukey post hoc multiple comparison test or a Kruskal-Wallis analysis followed by Dunn's post hoc multiple comparisons according to the normality of the distribution of the data. The significance threshold was set at $p < 0.05$.

3 | Results

3.1 | Histological Analysis of the DA Lesion

To analyze the extent of the DA lesion induced by the injection of 6-OHDA into the SNc in the animals used in the Western blot and Golgi-Cox experiments, we used TH immunohistochemistry. Similar to our previous experiments (Pautrat et al. 2023; Rolland et al. 2013), in addition to sham animals, two experimental groups were defined according to the extent of the DA

degeneration: partial and total DA lesion groups. The sham group received an injection of sterile saline unilaterally in the SNc instead of the toxin ($N=24$).

TH labeling in the SNc on the lesioned side in the partial DA lesion group was reduced to an average of $52.13 \pm 5.44\%$ (mean \pm standard error of the mean [SEM]) of the unlesioned side, with the remaining DA neurons located in the medial part of the SNc ($N=14$). In the total DA lesion group, only $13.16\% \pm 2.08\%$ (mean \pm SEM) of TH-labeled neurons remained in the lesioned SNc ($N=25$). The difference between these groups in terms of the percentage of the remaining TH labeling was statistically significant ($F(2, 60) = 174.4, p < 0.001$).

The survival of the nigral DA neurons was further analyzed by stereological counting of TH cells in the SNc. The analysis revealed a main effect of the lesion (Kruskal–Wallis, $K=39.99, p < 0.0001$, followed by Dunn's multiple comparisons test; number of TH cells, mean \pm SEM: sham = 422.80 ± 3.10 ; partial DA lesion: 166.50 ± 22.80 ; and total DA lesion: 57.33 ± 6.48).

Both methods reveal significant differences between the three experimental groups when considering the extent of 6-OHDA lesions in the SNc. The lesions have been illustrated in Figure S1.

3.2 | Golgi–Cox Analysis of Dendritic Spine Density and Morphology

Dendritic spines are a well-recognized locus of change when studying adaptive neuroplasticity (Risher et al. 2014; Trachtenberg et al. 2002). We have previously shown that partial and total DA lesion groups exhibit an increased density of dendritic spines in the PBN compared to sham, in particular an increase of filopodial and branched spine types (Pautrat et al. 2023). Given that the SC and PAG share the same connectivity with the basal ganglia as the PBN (for review, see Coizet et al. 2024), a similar change at the level of the spines was expected. Following Golgi–Cox staining in the SC and PAG, and using RECONSTRUCT, an average of $\sim 600 \mu\text{m}$ of dendrites was analyzed in each rat, according to the method developed by Risher et al. (2014). After counting and measuring the spines, the software categorized their morphology as filopodial, thin, long thin, stubby, mushroom, or branched (Figure 1). Here, we first present an analysis of the type of dendritic spines found in sham animals in the lateral SC, medial SC, and PAG, as to our

knowledge, this characterization had never been reported previously. As the analysis of the dendritic spine morphology in the PBN was not included in our previous work (Pautrat et al. 2023), we have also included it here for comparison. After an account of dendritic spine morphology in sham animals, next we analyzed the effect of DA lesions on the morphology of dendritic spines in the lateral SC, medial SC, and PAG.

3.2.1 | Morphology of Dendritic Spines in the Sham Group

3.2.1.1 | Lateral SC. We found a significant difference in the spine-type densities within the lateral SC of sham rats (Kruskal–Wallis, $K=175.2, p < 0.001$, followed by Dunn's multiple comparisons test, mean \pm SEM in Tables 1A and 1B). Overall, the dendritic spine morphology found in the lateral SC is largely of thin type (75%) and to a lesser extent stubby (15%) and long thin types (7.5%). Only a small proportion (1%–1.5%) of mushroom, filopodial, and branched types were found (Figure 2A).

3.2.1.2 | Medial SC. Similar to the lateral SC, analysis of the spine density and morphology in the sham group showed a significant difference in the density of the different spine types (Kruskal–Wallis, $K=156.7, p < 0.001$, followed by Dunn's multiple comparisons test, mean \pm SEM in Tables 1A and 1B). Overall, the dendritic spine morphology found in the medial SC is largely of thin type (74%) and to a lesser extent stubby (15%) and long thin types (6%). Only a small proportion (1%–3%) of mushroom, filopodial, and branched types were found (Figure 2B).

3.2.1.3 | PAG. Analysis of the spine morphology of sham animals also revealed a significant difference in the dendritic spine types (Kruskal–Wallis, $K=136.5, p < 0.001$, followed by Dunn's multiple comparisons test, mean \pm SEM in Tables 1A and 1B). The dendritic spine morphology found in the PAG is largely of thin type (74%) and to a lesser extent long thin (14%) and stubby types (9%). Again, only a small proportion (0.4%–2%) of mushroom, filopodial, and branched types were found (Figure 2C).

3.2.1.4 | PBN. Similarly to the SC and the PAG, analysis of the spine morphology of sham animals also revealed a significant difference in the dendritic spine types (Kruskal–Wallis,

TABLE 1A | Mean \pm SEM of the spine types in sham rats (Golgi–Cox, spines/ μm).

Golgi–Cox sham	Lateral SC	Medial SC	PAG
Mushroom	0.0019 ± 0.0008	0.0045 ± 0.0018	0.003 ± 0.0013
Filopodial	0.002 ± 0.001	0.0053 ± 0.0019	0.002 ± 0.001
Branched	0.0054 ± 0.0017	0.0157 ± 0.0028	0.011 ± 0.003
Long thin	0.0289 ± 0.005	0.0278 ± 0.0056	0.065 ± 0.008
Stubby	0.0586 ± 0.0075	0.071 ± 0.0081	0.040 ± 0.008
Thin	0.289 ± 0.0147	0.355 ± 0.021	0.341 ± 0.019
Units	Mean \pm SEM—spines/ μm		

TABLE 1B | Mean \pm SEM of the spine density and spine types (Golgi–Cox, spines/ μ m) and GABA_A receptor expression (Western blot, GABA_A/GAPDH ratio) according to the structures and the experimental groups analyzed.

Impact of DA lesion	Lateral SC			Medial SC			PAG		
	Sham	Partial	Total	Sham	Partial	Total	Sham	Partial	Total
Golgi–Cox									
Density	0.389 \pm 0.018	0.3471 \pm 0.017	0.595 \pm 0.0284	0.490 \pm 0.021	0.520 \pm 0.0391	0.780 \pm 0.038	0.463 \pm 0.0261	0.451 \pm 0.023	0.743 \pm 0.0326
Thin	0.289 \pm 0.0147	0.282 \pm 0.0177	0.398 \pm 0.02	0.355 \pm 0.021	0.383 \pm 0.028	0.535 \pm 0.032	0.341 \pm 0.019	0.354 \pm 0.022	0.490 \pm 0.023
Stubby	0.0586 \pm 0.0075	0.0285 \pm 0.0038	0.123 \pm 0.0151	0.071 \pm 0.0081	0.051 \pm 0.010	0.143 \pm 0.010	0.040 \pm 0.008	0.0284 \pm 0.006	0.160 \pm 0.0136
Mushroom	0.0019 \pm 0.0008	0.007 \pm 0.0026	0.009 \pm 0.0025	0.0045 \pm 0.0018	0.0055 \pm 0.0026	0.014 \pm 0.003	0.003 \pm 0.0013	0.006 \pm 0.0017	0.105 \pm 0.0027
Units									
Western blot									
GABA _A	0.082 \pm 0.011	0.083 \pm 0.01	0.119 \pm 0.011	0.14 \pm 0.035	0.16 \pm 0.052	0.15 \pm 0.032	0.156 \pm 0.008	0.174 \pm 0.016	0.195 \pm 0.017
Units									

Mean \pm SEM—spines/ μ m

GABA_A/GAPDH ratio

$K=60.91$, $p<0.001$, followed by Dunn's multiple comparisons test, number of cells: mean \pm SEM). However, the dendritic spine morphology found in the PBN is differently distributed compared to the SC and the PAG with a majority of mushroom (36%), thin (23%), and stubby (19%) types. Again, a smaller proportion (5%–9%) of long thin, filopodial, and branched types were found (Figure 2D).

3.2.2 | Effect of DA Lesions on Dendritic Spines

3.2.2.1 | Lateral SC. The statistical analysis comparing sham and DA lesioned rats revealed a significant increase in the spine density in the total DA lesion group compared to both the sham and partial DA lesion groups (Kruskal–Wallis, $K=44.93$, followed by Dunn's multiple comparisons test, $p<0.001$). Further analysis of the spine morphology showed a significant increase of the thin spine type in the total DA lesion group compared to both the sham and partial DA lesion groups (ANOVA, $F(2, 113)=13.82$, followed by Tukey's multiple comparisons test, $p<0.001$). The differences between the sham and partial DA lesion groups were not statistically significant.

This analysis also revealed a significant change in the density of the stubby spine type (Kruskal–Wallis, $K=36.41$, followed by Dunn's multiple comparisons test, $p<0.001$). The extent of the DA lesion produced substantially different outcomes, with a significant decrease of this spine type in the partial DA group (partial DA lesion group vs. sham, $p<0.05$; partial DA lesion group vs. total DA lesion group, $p<0.001$) and an increase in this spine type in the total DA group (total DA lesion group vs. sham, $p<0.05$). A trend toward an increase of the mushroom spine-type density was also found in both DA lesion groups (Kruskal–Wallis, $K=4.767$, followed by Dunn's multiple comparisons test, $p=0.09$). The other types of spines were not changed by the DA lesion (branched, filopodial, and long thin) (Figure 3A,D, mean \pm SEM in Tables 1A and 1B).

3.2.2.2 | Medial SC. Statistical analysis of the medial SC revealed a significant increase in the spine density in the total DA lesion group when compared to both the sham and partial DA lesion groups (Kruskal–Wallis, $K=34.69$, followed by Dunn's multiple comparisons test, $p<0.001$). We found a significant increase in thin (Kruskal–Wallis, $K=17.99$, followed by Dunn's multiple comparisons test, $p<0.001$), stubby (Kruskal–Wallis, $K=41.28$, followed by Dunn's multiple comparisons test, $p<0.001$), and mushroom-type spine density (Kruskal–Wallis, $K=7.97$, followed by Dunn's multiple comparisons test, $p<0.05$) in the total DA lesion group compared to both the sham and partial DA lesion groups. The differences between the sham and partial DA lesion groups were not statistically significant. The other types of spine morphology were not altered by the DA lesion (Figure 3B,E, mean \pm SEM in Tables 1A and 1B).

3.2.2.3 | PAG. Similar to the lateral SC, statistical analysis showed a significant increase in spine density in the PAG in the total DA lesion group only (Kruskal–Wallis, $K=40.38$, followed by Dunn's multiple comparisons test, $p<0.001$). Analysis of the spine morphology revealed a significant increase of the thin

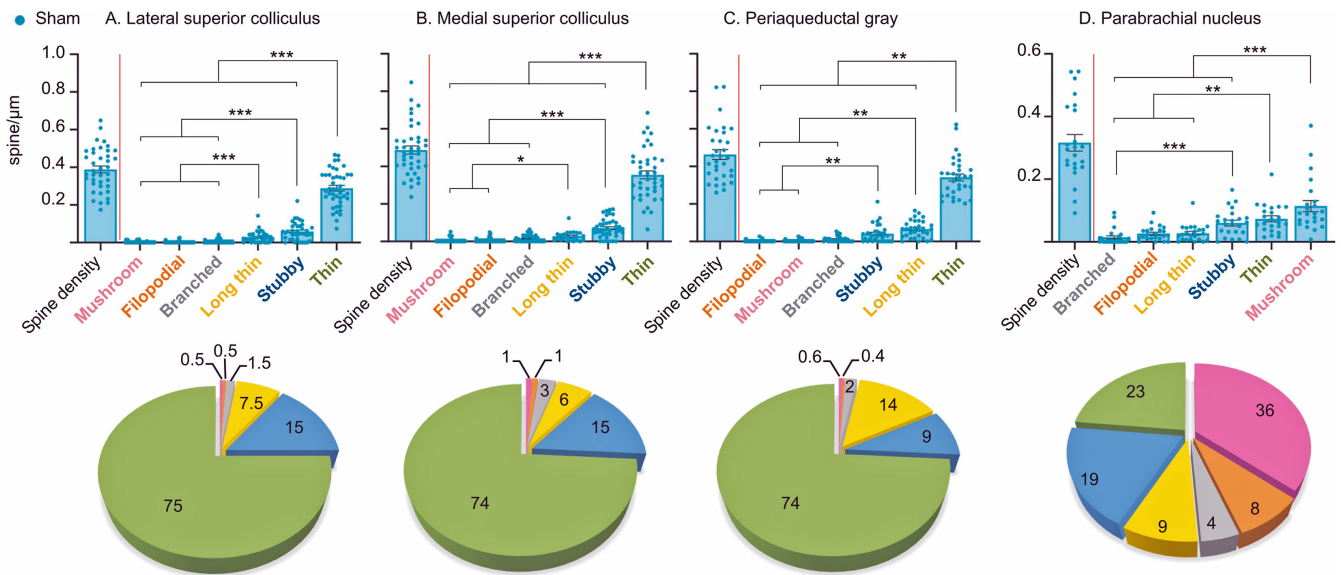


FIGURE 2 | Histograms (mean ± SEM) (top panels) and pie charts (bottom panels) of the proportion of the dendritic spine morphologies measured in the sham group in the lateral superior colliculus (A), the medial superior colliculus (B), the periaqueductal gray (C), and the parabrachial nucleus (D) in relation to the total spine density of these structures. The dendritic spine types were classified as mushroom (pink), filopodial (orange), branched (gray), long thin (yellow), stubby (dark blue), and thin (green). * $p < 0.05$, ** $p < 0.01$, and *** $p < 0.001$.

(Kruskal–Wallis, $K = 22.05$, followed by Dunn's multiple comparisons test, $p < 0.001$) and stubby (Kruskal–Wallis, $K = 52.68$, followed by Dunn's multiple comparisons test, $p < 0.001$) spine types in the total DA lesion group compared to both the sham and partial DA lesion groups. The differences between the sham and partial DA lesion groups were not statistically significant. A trend toward a significant increase of the mushroom spine type is also found (Kruskal–Wallis, $K = 5.174$, followed by Dunn's multiple comparisons test, $p = 0.07$) (Figure 3C,F, mean ± SEM in Tables 1A and 1B).

3.3 | Western Blot Analysis of GABA_A Receptor Expression

The second parameter of adaptive neuroplasticity that we investigated was the potential change in GABA receptor expression as a consequence of increased activity in SNr projections to the SC and the PAG following DA denervation. The GABA_A receptor is the most common receptor at inhibitory synapses such as those present between the SNr and the SC/PAG (Oertel and Mugnaini 1984), and we have previously found total DA lesions to lead to increased levels of GABA_A receptors in the PBN (Pautrat et al. 2023). Western blot analysis was therefore used to detect and compare the possible change in GABA_A receptor expression in the SC and the PAG between the three experimental groups.

3.3.1 | Lateral SC

In this experiment, we compared the sham ($n = 9$), partial ($n = 9$), and total ($n = 11$) DA lesion groups in terms of GABA_A receptor expression in the lateral SC. A significant increase of GABA_A receptor expression was found in the total DA lesion group compared to the sham and partial DA lesion groups (ANOVA,

$F(2, 23) = 3.843$, $p < 0.05$) (Figure 4A, mean ± SEM in Tables 1A and 1B).

3.3.2 | Medial SC

We also compared the sham ($n = 15$), partial ($n = 9$), and total ($n = 15$) DA lesion groups in relation to the medial SC. Unlike the lateral SC, analysis of the GABA_A receptor expression in the medial part of the SC did not show a statistical difference between the experimental groups (ANOVA, $F(2, 36) = 0.022$, $p = 0.97$) (Figure 4B, mean ± SEM in Tables 1A and 1B).

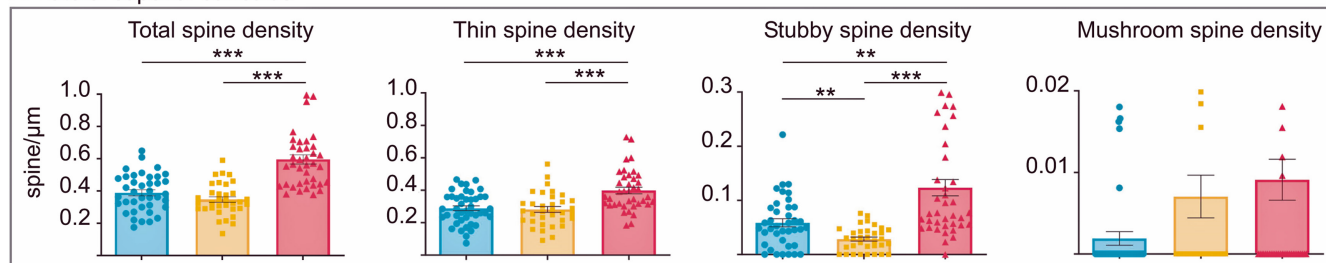
3.3.3 | PAG

Finally, we compared sham ($n = 7$), partial ($n = 9$), and total ($n = 9$) DA lesion groups in relation to the PAG. Similar to the medial SC, analysis of the GABA_A receptor expression in the PAG did not show a statistical difference between the experimental groups (ANOVA, $F(2, 22) = 1.501$, $p = 0.2449$) (Figure 4C, mean ± SEM in Tables 1A and 1B).

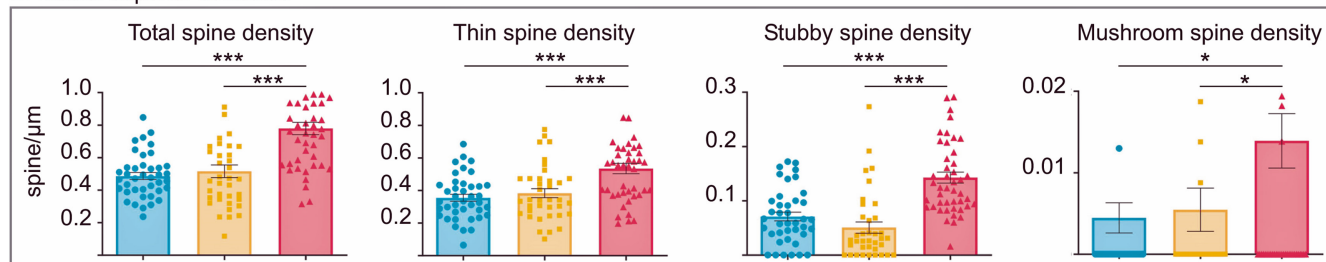
4 | Discussion

We previously described the presence of neuroplasticity at the level of the density of dendritic spines and expression of GABA_A receptors within the PBN in two rat models of PD with partial or total DA degeneration in the SNc (Pautrat et al. 2023). With the SC and the PAG sharing the same connectivity with the basal ganglia as the PBN and the hyperactivity of SNr GABAergic projections to the SC and PAG in the context of PD, we expected that a similar change would be found within these structures in the same rat models of PD—this issue has never been studied previously. However,

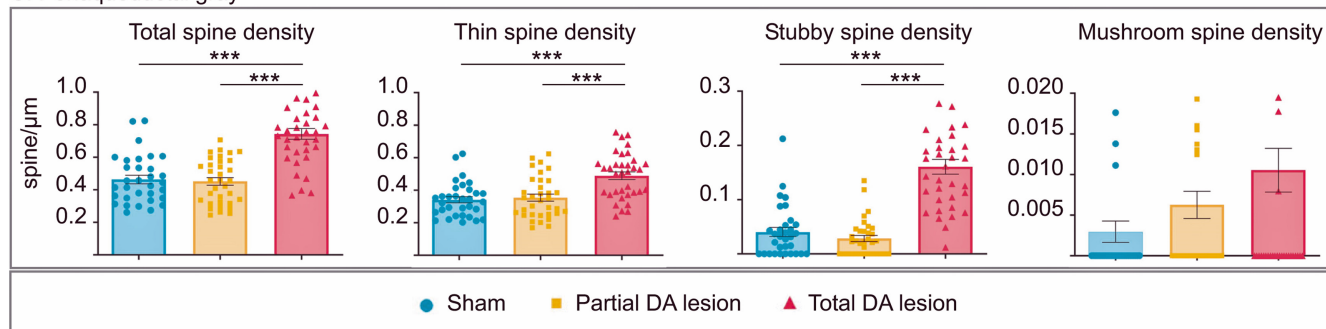
A. Lateral superior colliculus



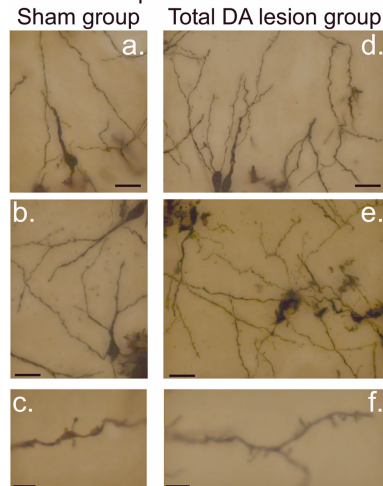
B. Medial superior colliculus



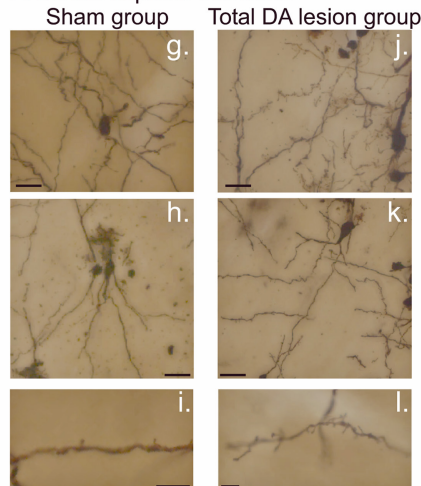
C. Periaqueductal gray



D. Lateral superior colliculus



E. Medial superior colliculus



F. Periaqueductal gray

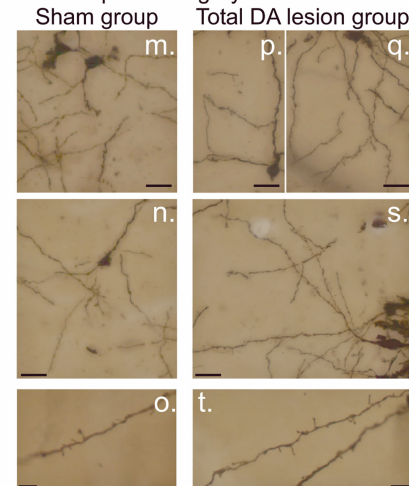


FIGURE 3 | Top panel: histograms (mean \pm SEM) of the total spine, thin spine, stubby spine, and mushroom spine density measured in tissue labeled with Golgi-Cox staining in the sham (blue), partial (orange), and total (red) DA lesion groups within the lateral superior colliculus (A), the medial superior colliculus (B), and the periaqueductal gray (C). Bottom panel: photomicrograph montages (merge of different Z axes) of dendritic spines labeled with Golgi-Cox staining in the lateral superior colliculus (D), the medial superior colliculus (E), and the periaqueductal gray (F) in the sham (a–c, g–i, m–o) and total DA lesion groups (d–f, j–l, p, q, s, t). Scale bar = 20 μm (top and middle pictures). Scale bar = 5 μm (bottom pictures). * $p < 0.05$, ** $p < 0.01$, and *** $p < 0.001$.

unlike the PBN, the overall spine density was largely unaffected in the partial DA lesion group in both the SC and the PAG. However, the total DA lesion group showed an increase

in spine density in the medial and lateral SCs and in the PAG. An increase in GABA_A receptor expression was also found in the lateral SC in this group.

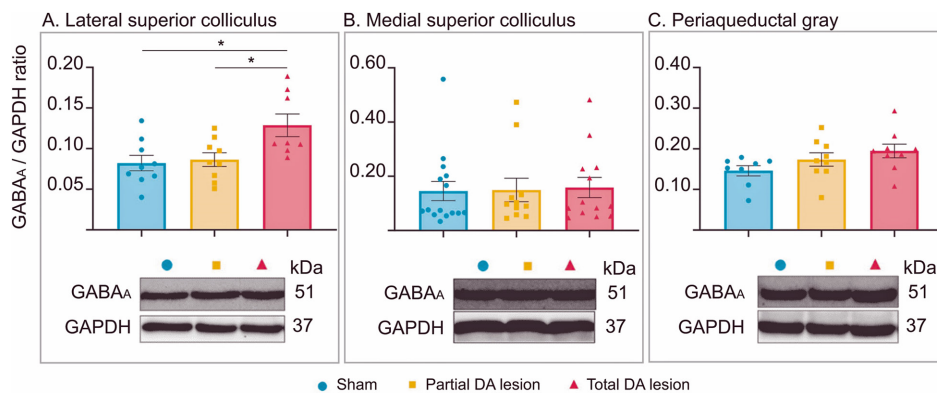


FIGURE 4 | Histograms of GABA_A/GAPDH ratio (mean ± SEM) (top panels) and individual examples of Western blot immuno-expression against GABA protein and GAPDH as a protein migration control (bottom panels) measured using Western blot in the sham (blue), partial (orange), and total (red) DA lesion groups within the lateral superior colliculus (A), the medial superior colliculus (B), and the periaqueductal gray (C). **p* < 0.05.

4.1 | Functional Implications of Spine Morphology

Most of the literature on dendritic spines concerns the cortex or the hippocampus, within which spine genesis, function, and dynamics remain a topic of discussion (Pchitskaya and Bezprozvanny 2020; Rasia-Filho et al. 2023). Spines on neurons in subcortical structures have received comparatively little attention, and it is instructive to consider the functional implications of our findings. It has been suggested that the function of dendritic spines is not simply linked to the size of the dendritic surface available for synaptic contacts. Using a computational approach, Segev and Rall (1988, 1998) proposed that the width of the spine neck influences its electrical resistance, thereby affecting the extent to which synaptic inputs on the spine influence the somatic membrane potential. Thin spine necks will increase the spine stem resistance, leading to large local excitatory (EPSPs) and inhibitory postsynaptic potentials (IPSPs) at the level of the spine head. These may have comparatively little effect on the somatic membrane potential and hence the likelihood of spike activity. However, we also found that stubby spine densities are strongly increased in these structures, especially in the PAG. Stubby spines have a large head, similarly to mushroom spines, and no obvious constriction between the head and the attachment to the shaft. A wider spine stem might be expected to reduce local EPSPs and IPSPs in the spine head, although due to decreased resistance, those local potentials are likely to influence spike activity in a way that the corresponding potentials in thin spines would not.

4.2 | Impact of Dendritic Spine Morphology on Plasticity

At the level of the dendritic spines, it is interesting to note several discrepancies between these midbrain structures, the SC/PAG, and the PBN, located at the junction between the pons and the midbrain. In both the PAG and the SC (whether the medial or the lateral regions), the majority of spines have a thin-type morphology, and to a lesser extent, stubby and long thin morphology. Unlike the SC/PAG, the majority of spines in the PBN have a mushroom-type morphology, followed by thin and stubby types. Following a DA lesion in the SNC, these

types of spines in the PBN remained stable, but branched and filopodial types increased in density (Pautrat et al. 2023), whereas in the SC and PAG, thin and stubby spine densities increased. The morphology of the spines may thus represent an important factor underlying plasticity in a pathological context.

4.3 | Impact of Increased GABA_A Receptor Expression

We and others have previously shown that DA lesions lead to an elevation in the firing rate of neurons in the SNr (Breit et al. 2006; Diaz et al. 2003; Pautrat et al. 2023; Waszczak and Walters 1984), which will increase inhibitory tone in structures receiving an input from the SNr. Postsynaptic plasticity following repeated presynaptic activation has previously been associated not only with an increase in excitatory synapses but also in GABAergic synapses on spines (Knott et al. 2002; Mele et al. 2016), which the increase in GABA_A receptor expression that we report suggests may be happening in the lateral SC. Furthermore, it has also been shown at the level of the hippocampus that long-term potentiation (LTP), an electrophysiological model of neuronal plasticity, is associated with enlargement of the spine head and shortening of the spine neck or the induction of short, stubby spines and thus changes in synaptic strength and EPSPs (see Rasia-Filho et al. 2023 for review). With the significant increase of stubby spines following a DA lesion in the SC and PAG, the potential presence of LTP implies that these changes at the level of the spines are likely to become long-lasting in the context of PD. Evidence of the presence of LTP is further supported, at least in the lateral SC, by our finding of increased GABA_A receptor levels in this part of the SC. Indeed, GABA_A receptors mediate fast synaptic inhibition by controlling rapid chloride ion flow, which is critical for the timing and modulation of synaptic strength. This rapid response is essential for LTP and LTD at inhibitory synapses (Chiu et al. 2019). It has been shown at the level of the hippocampus that increased numbers of synaptic GABA_A receptors underlie potentiation of GABAergic neurotransmission in this structure (Nusser et al. 1998). This raises the possibility that postsynaptic insertion of new GABA_A receptors in the lateral SC may increase the efficacy of inhibitory synapses underlying long-lasting and marked alteration of synaptic transmission.

The limitation of GABA_A receptor changes to the medial SC may come down to the fact that the nigrothalamic pathway heavily projects to the lateral part of the SC and to a lesser extent to the medial regions of this structure (Harting et al. 1988). Note that the effect of increased GABA_A receptors in the lateral SC may not be restricted to neurons alone. Astrocytes express ionotropic GABA_A receptors and are thus “GABA-receptive cells,” at least in the thalamus, hippocampus, and cerebellum (Jiménez-González et al. 2011; Lee et al. 2010; Wang et al. 2024). It has been proposed that GABA_A receptors expressed in astrocytes could also play a role in maintaining inhibitory tone and supporting neuroplasticity, such as the increase in stubby and thin spine types we observed. Furthermore, it has been shown that microglia play a variety of roles in synaptic plasticity. One such role includes synapse elimination via phagocytosis (Andoh and Koyoma 2021).

4.4 | Neuroplasticity and SNr Connectivity

We found a discrepancy between the SC/PAG and the PBN in terms of the effect of the extent of the DA lesion on dendritic spine neuroplasticity. Within the PBN, a partial DA lesion in the SNc was found to be enough to induce an increase in spine density similar to that found following a total DA lesion (Pautrat et al. 2023). However, that was not the case for the SC (whether the medial or the lateral part) or the PAG, where a total DA lesion was required to change spine density. This result is surprising at the level of the SC because both partial and total DA lesions produce a visual sensory rebound in the SC measured electrophysiologically (Rolland et al. 2013), similarly to the PBN with noxious stimuli (Pautrat et al. 2023). This could suggest that other types of neuroplasticity, not studied in our work, may be found within the SC and PAG of animals with partial DA lesions, which should be explored further.

The possibility exists that the differences we have found between the internal micro-organization of each structure studied may also come down to the type and strength of the SNr projections onto the SC/PAG and PBN. Cumulative evidence from the literature refutes the classical assumption of the neurochemically and neuroanatomically homogeneous nature of the SNr. An early study described the SNr as containing both GAD-positive and GAD-negative cells (Oertel and Mugnaini 1984). Kha et al. (2001) then highlighted the diversity of neurochemicals within the SNr, with neurons reactive to antibodies against GABA, glutamate, choline acetyltransferase, and the vesicular acetylcholine transporter. Note that glutamate is the metabolic precursor of GABA. Therefore, immunoreactivity for glutamate should not be taken as an indication of the presence of glutamatergic neurons among a large population of GABAergic neurons. This is coherent with the finding that the SNr provides an output to the thalamic nucleus reticularis with an excitatory component in parallel with the classical inhibitory output to the ventroposterolateral nucleus and both excitatory and inhibitory output to the posterior nucleus of the thalamus (Antal et al. 2014). A similar variability of SNr influence may also be found for the brainstem structures. Anatomically, McElvain et al. (2021) recently found that the SNr contained distinct pools of neuronal projections differentially targeting structures from the brainstem, each pool having specific electrophysiological properties.

A subset of SNr neurons targets the lateral SC, which differs from the subset targeting the medial SC, the PAG, and the PBN (McElvain et al. 2021). In addition to these physiological data, it has been shown that a DA lesion differentially impacts SNr neurons according to their nature (Delgado-Zabalza et al. 2023). Parvalbumin-positive neuronal firing rate is altered, but not parvalbumin-negative neurons. Altogether, these data from the literature highlight that the link between the SNr and its targets is more complex than originally thought, with a larger diversity of projections in terms of cell type, physiology, and strength.

5 | Limitations

We feel it is important to briefly draw attention to a couple of limitations in the present work. Our analysis indicates a strong plasticity at the level of the dendritic spines, with an increase of thin and stubby spine types within the SC and PAG in animals with a total DA lesion and increased GABA_A receptor expression in this group in the lateral SC. However, our analysis was performed 3 weeks after the lesion, and we cannot exclude the possibility that additional changes to these parameters may have occurred after a longer delay. Furthermore, changes observed might also represent an early stage of plasticity that may not persist in time.

The structural changes found at the level of the dendritic spines and the changes in receptor expression suggest that synapses themselves may be altered, although this has not been assessed in the present work. Additional experiments using electron microscopy should now be performed to fully evaluate the shape of the postsynaptic density following DA lesions, which we have shown to be reduced in the PBN (Pautrat et al. 2023) and may further impact synaptic transmission. Electrophysiological experiments are also crucial to perform to assess changes in synaptic strength. We also cannot exclude the possibility of additional neuroplasticity impacting the glutamatergic system with glutamatergic synapses located on the head of the spines. Overall, neuroplasticity mechanisms within the brainstem, a major direct target of the basal ganglia, to our knowledge, have hardly been studied before. Our previous work (Pautrat et al. 2023), in addition to the present experiments, provides the first evidence of such a mechanism in the PBN, SC, and PAG in the context of PD. Finer analysis is now needed to compare anatomical and structural changes in neurons directly connected with the SNr with those that are not connected to fully confirm the impact of the SNr in the neuroplasticity observed in our regions of interest. We also have based our analysis on the anatomical and molecular plasticity occurring within the SC and the PAG but not the functional consequences of that plasticity in terms of the development of nonmotor symptoms in PD such as attentional deficits or pain symptoms, in which the SC and the PAG could be involved, respectively (Basso et al. 2021; Tovote et al. 2016).

Finally, as reviewed by Rasia-Filho et al. (2023), human dendritic spines are similar in shape when compared to other animals, but dendritic spines have reached higher levels of complexity in humans. Human spines show a diverse shape spectrum compared to other species; thus, care should be taken in extrapolating our results in a clinical context, and a specific analysis of human tissue is crucial to confirm such mechanisms on PD.

6 | Conclusion

In conclusion, the connectivity between the SNr and other brainstem nuclei is poorly characterized and understood. Earlier, we have shown that structures such as the SC and the PBN exhibit altered sensory processing following the degeneration of DA neurons (Pautrat et al. 2023; Rolland et al. 2013), and in the present work, the SC and PAG, similarly to the PBN (Pautrat et al. 2023), showed an internal anatomical reorganization. Further work is required to explore in more detail the link between the basal ganglia and the brainstem, especially at the level of the SNr output, to fully evaluate the functional impact PD could generate in these structures.

Author Contributions

Racha Al Tannir: conceptualization, formal analysis, investigation, methodology, writing – original draft. **Arnaud Pautrat:** formal analysis, methodology. **Remi Soutrenon:** investigation. **Paul G. Overton:** writing – review and editing. **Veronique Coizet:** conceptualization, formal analysis, methodology, writing – review and editing.

Acknowledgments

We thank the personnel from the animal facility for their technical contributions. This work was supported by the Photonic Imaging Center of Grenoble Institut des Neurosciences (Université Grenoble Alpes—Inserm U1216), which is part of the ISdV core facility and certified by the IBI SA label.

Conflicts of Interest

The authors declare no conflicts of interest.

Data Availability Statement

The data that support the findings of this study are available from the corresponding author upon request.

Peer Review

The peer review history for this article is available at <https://www.webofscience.com/api/gateway/wos/peer-review/10.1111/ejn.70068>.

References

- Albin, R. L., A. B. Young, and J. B. Penney. 1989. “The Functional Anatomy of Basal Ganglia Disorder.” *Trends in Neurosciences* 12, no. 10: 366–375. [https://doi.org/10.1016/0166-2236\(89\)90074-x](https://doi.org/10.1016/0166-2236(89)90074-x).
- Andoh, M., and R. Koyoma. 2021. “Microglia Regulate Synaptic Development and Plasticity.” *Developmental Neurobiology* 81, no. 5: 568–590.
- Antal, M., B. M. Beneduce, and W. G. Regehr. 2014. “The Substantia Nigra Conveys Target-Dependent Excitatory and Inhibitory Outputs From the Basal Ganglia to the Thalamus.” *Journal of Neuroscience* 34, no. 23: 8032–8042. <https://doi.org/10.1523/JNEUROSCI.0236-14.2014>.
- Arkadir, D., H. Bergman, and S. Fahn. 2014. “Redundant Dopaminergic Activity May Enable Compensatory Axonal Sprouting in Parkinson Disease.” *Neurology* 82, no. 12: 1093–1098. <https://doi.org/10.1212/WNL.0000000000000243>.
- Basso, M. A., M. E. Bickford, and J. Cang. 2021. “Unraveling Circuits of Visual Perception and Cognition Through the Superior Colliculus.” *Neuron* 109, no. 6: 918–937. <https://doi.org/10.1016/j.neuron.2021.01.013>.

- Bergman, H., T. Wichmann, B. Karmon, and M. DeLong. 1994. “The Primate Subthalamic Nucleus. II. Neuronal Activity in the MPTP Model of Parkinsonism.” *Journal of Neurophysiology* 72, no. 2: 507–520. <https://doi.org/10.1152/jn.1994.72.2.507>.
- Bezard, E., and C. E. Gross. 1998. “Compensatory Mechanisms in Experimental and Human Parkinsonism: Towards a Dynamic Approach.” *Progress in Neurobiology* 55, no. 2: 93–116. [https://doi.org/10.1016/s0301-0082\(98\)00006-9](https://doi.org/10.1016/s0301-0082(98)00006-9).
- Blesa, J., I. Trigo-Damas, M. Dileone, N. Del Lopez-Gonzalez Rey, L. F. Hernandez, and J. A. Obeso. 2017. “Compensatory Mechanisms in Parkinson's Disease: Circuits Adaptations and Role in Disease Modification.” *Experimental Neurology* 298, no. Pt B: 148–161. <https://doi.org/10.1016/j.expneurol.2017.10.002>.
- Blesa, J., I. Trigo-Damas, and J. A. Obeso. 2016. “Parkinson's Disease and Thalamus: Facts and Fancy.” *Lancet Neurology* 15, no. 7: e2. [https://doi.org/10.1016/S1474-4422\(16\)30048-5](https://doi.org/10.1016/S1474-4422(16)30048-5).
- Breit, S., L. Lessmann, D. Unterbrink, R. C. Popa, T. Gasser, and J. B. Schulz. 2006. “Lesion of the Pedunculopontine Nucleus Reverses Hyperactivity of the Subthalamic Nucleus and Substantia Nigra Pars Reticulata in a 6-Hydroxydopamine Rat Model.” *European Journal of Neuroscience* 24: 2275–2282. <https://doi.org/10.1111/j.1460-9568.2006.05106.x>.
- Carpenter, M. B. 1976. “Anatomy of the Basal Ganglia and Related Nuclei: A Review.” *Advances in Neurology* 14: 7–48.
- Chiu, C. Q., A. Barberis, and M. J. Higley. 2019. “Preserving the Balance: Diverse Forms of Long-Term GABAergic Synaptic Plasticity.” *Nature Reviews Neuroscience* 20, no. 5: 272–281. <https://doi.org/10.1038/s41583-019-0141-5>.
- Clavier, R. M., S. Atmadja, and H. C. Fibiger. 1976. “Nigrothalamic Projections in the Rat as Demonstrated by Orthograde and Retrograde Tracing Techniques.” *Brain Research Bulletin* 1, no. 4: 379–384. [https://doi.org/10.1016/0361-9230\(76\)90031-9](https://doi.org/10.1016/0361-9230(76)90031-9).
- Coizet, V., R. Al Tannir, A. Pautrat, and P. G. Overton. 2024. “Separation of Channels Subserving Approach and Avoidance/Escape at the Level of the Basal Ganglia and Related Brainstem Structures.” *Current Neuropharmacology* 22, no. 9: 1473–1490. <https://doi.org/10.2174/1570159X21666230818154903>.
- Delgado-Zabalza, L., N. P. Mallet, C. Glangetas, et al. 2023. “Targeting Parvalbumin-Expressing Neurons in the Substantia Nigra Pars Reticulata Restores Motor Function in Parkinsonian Mice.” *Cell Reports* 42, no. 10: 113287. <https://doi.org/10.1016/j.celrep.2023.113287>.
- Deniau, J. M., and G. Chevalier. 1992. “The Lamellar Organization of the Rat Substantia Nigra Pars Reticulata: Distribution of Projection Neurons.” *Neuroscience* 46, no. 2: 361–377. [https://doi.org/10.1016/0306-4522\(92\)90058-a](https://doi.org/10.1016/0306-4522(92)90058-a).
- Diaz, M. R., P. Barroso-Chinea, A. Acevedo, and T. Gonzalez-Hernandez. 2003. “Effects of Dopaminergic Cell Degeneration on Electrophysiological Characteristics and GAD65/GAD67 Expression in the Substantia Nigra: Different Action on GABA Cell Subpopulations.” *Movement Disorders* 18: 254–266. <https://doi.org/10.1002/mds.10345>.
- Fiala, J. C. 2005. “Reconstruct: A Free Editor for Serial Section Microscopy.” *Journal of Microscopy* 218: 52–61. [https://doi.org/10.1016/0165-0270\(80\)90021-7](https://doi.org/10.1016/0165-0270(80)90021-7).
- Harting, J. K., M. F. Huerta, T. Hashikawa, J. T. Weber, and D. P. van Lieshout. 1988. “Neuroanatomical Studies of the Nigrotectal Projection in the Cat.” *Journal of Comparative Neurology* 278, no. 4: 615–631. <https://doi.org/10.1002/cne.902780412>.
- Hassani, O., M. Mouroux, and J. Féger. 1996. “Increased Subthalamic Neuronal Activity After Nigral Dopaminergic Lesion Independent of Disinhibition via the Globus Pallidus.” *Neuroscience* 72, no. 1: 105–115. [https://doi.org/10.1016/0306-4522\(95\)00535-8](https://doi.org/10.1016/0306-4522(95)00535-8).
- Hopkins, D. A., and L. W. Niessen. 1976. “Substantia Nigra Projections to the Reticular Formation, Superior Colliculus and Central Gray in the

- Rat, Cat and Monkey." *Neuroscience Letters* 2, no. 5: 253–259. [https://doi.org/10.1016/0304-3940\(76\)90156-7](https://doi.org/10.1016/0304-3940(76)90156-7).
- Jiménez-González, C., T. Pirttimäki, D. W. Cope, and H. R. Parri. 2011. "Non-Neuronal, Slow GABA Signalling in the Ventrobasal Thalamus Targets δ -Subunit-Containing GABA_A Receptors." *European Journal of Neuroscience* 33: 1482–2011. <https://doi.org/10.1111/j.1460-9568.2011.07645.x>.
- Kha, H. T., D. I. Finkelstein, D. Tomas, D. Drago, D. V. Pow, and M. K. Horne. 2001. "Projections From the Substantia Nigra Pars Reticulata to the Motor Thalamus of the Rat: Single Axon Reconstructions and Immunohistochemical Study." *Journal of Comparative Neurology* 440, no. 1: 20–30. <https://doi.org/10.1002/cne.1367>.
- Knott, G. W., C. Quairiaux, C. Genoud, and E. Welker. 2002. "Formation of Dendritic Spines With GABAergic Synapses Induced by Whisker Stimulation in Adult Mice." *Neuron* 34, no. 2: 265–273. [https://doi.org/10.1016/s0896-6273\(02\)00663-3](https://doi.org/10.1016/s0896-6273(02)00663-3).
- Lee, S., B.-E. Yoon, K. Berglund, et al. 2010. "Channel-Mediated Tonic GABA Release From Glia." *Science* 330: 790–796. <https://doi.org/10.1126/science.1184334>.
- McElvain, L. E., Y. Chen, J. D. Moore, et al. 2021. "Specific Populations of Basal Ganglia Output Neurons Target Distinct Brain Stem Areas While Collateralizing Throughout the Diencephalon." *Neuron* 109, no. 10: 1721–1738. <https://doi.org/10.1016/j.neuron.2021.03.017>.
- Mele, M., G. Leal, and C. Duarte. 2016. "Role of GABA_A Trafficking in the Plasticity of Inhibitory Synapses." *Journal of Neurochemistry* 139, no. 6: 997–1018. <https://doi.org/10.1111/jnc.13742>.
- Mink, J. W. 1996. "The Basal Ganglia: Focused Selection and Inhibition of Competing Motor Programs." *Progress in Neurobiology* 50: 381–425. [https://doi.org/10.1016/s0301-0082\(96\)00042-1](https://doi.org/10.1016/s0301-0082(96)00042-1).
- Moro, E., E. Bellot, S. Meoni, et al. 2020. "Visual Dysfunction of the Superior Colliculus in De Novo Parkinsonian Patients." *Annals of Neurology* 87, no. 4: 533–546. <https://doi.org/10.1002/ana.25696>.
- Nusser, Z., N. Hájos, P. Somogyi, and I. Mody. 1998. "Increased Number of Synaptic GABA_A Receptors Underlies Potentiation at Hippocampal Inhibitory Synapses." *Nature* 395, no. 6698: 172–177. <https://doi.org/10.1038/25999>.
- Oertel, W. H., and E. Mugnaini. 1984. "Immunocytochemical Studies of GABAergic Neurons in Rat Basal Ganglia and Their Relations to Other Neuronal Systems." *Neuroscience Letters* 47, no. 3: 233–238. [https://doi.org/10.1016/0304-3940\(84\)90519-6](https://doi.org/10.1016/0304-3940(84)90519-6).
- Pahapill, P. A., and A. M. Lozano. 2000. "The Pedunculopontine Nucleus and Parkinson's Disease." *Brain* 123, no. Pt 9: 1767–1783. <https://doi.org/10.1093/brain/123.9.1767>.
- Pautrat, A., R. Al Tannir, K. Pernet-Galley, et al. 2023. "Altered Parabrachial Nucleus Nociceptive Processing May Underlie Central Pain in Parkinson's Disease." *npj Parkinson's Disease* 9, no. 1: 78. <https://doi.org/10.1038/s41531-023-00516-x>.
- Paxinos, G., and C. Watson. 2007. *The Rat Brain in Stereotaxic Coordinates*. Sydney: Academic Press.
- Pchitskaya, E., and I. Bezprozvanny. 2020. "Dendritic Spines Shape Analysis—Classification or Clusterization? Perspective." *Frontiers in Synaptic Neuroscience* 12: 31. <https://doi.org/10.3389/fnsyn.2020.00031>.
- Rasia-Filho, A. A., M. E. Calcagnotto, U. von Bohlen, and O. Halbach. 2023. "Introduction: What Are Dendritic Spines?" *Advances in Neurology* 34: 1–68. https://doi.org/10.1007/978-3-031-36159-3_1.
- Redgrave, P., T. J. Prescott, and K. Gurney. 1999. "The Basal Ganglia: A Vertebrate Solution to the Selection Problem?" *Neuroscience* 89, no. 4: 1009–1023. [https://doi.org/10.1016/s0306-4522\(98\)00319-4](https://doi.org/10.1016/s0306-4522(98)00319-4).
- Redgrave, P., M. Rodriguez, Y. Smith, et al. 2010. "Goal-Directed and Habitual Control in the Basal Ganglia: Implications for Parkinson's Disease." *Nature Reviews Neuroscience* 11, no. 11: 760–772. <https://doi.org/10.1038/nrn2915>.
- Risher, W., T. Ustunkaya, J. Alvarado, and C. Eroglu. 2014. "Rapid Golgi Analysis Method for Efficient and Unbiased Classification of Dendritic Spines." *PLoS ONE* 9, no. 9: e107591. <https://doi.org/10.1371/journal.pone.0107591>.
- Rolland, M., C. Carcenac, P. Overton, M. Savasta, and V. Coizet. 2013. "Enhanced Visual Responses in the Superior Colliculus and Subthalamic Nucleus in an Animal Model of Parkinson's Disease." *Neuroscience* 252: 277–288. <https://doi.org/10.1016/j.neuroscience.2013.07.047>.
- Schneider, J. 1986. "Interactions Between the Basal Ganglia, the Pontine Parabrachial Region, and the Trigeminal System in Cat." *Neuroscience* 19, no. 2: 411–425. [https://doi.org/10.1016/0306-4522\(86\)90271-x](https://doi.org/10.1016/0306-4522(86)90271-x).
- Segev, I., and W. Rall. 1988. "Computational Study of an Excitable Dendritic Spine." *Journal of Neurophysiology* 60, no. 2: 499–523. <https://doi.org/10.1152/jn.1988.60.2.499>.
- Segev, I., and W. Rall. 1998. "Excitable Dendrites and Spines: Earlier Theoretical Insights Elucidate Recent Direct Observations." *Trends in Neurosciences* 21, no. 11: 453–460. [https://doi.org/10.1016/s0166-2236\(98\)01327-7](https://doi.org/10.1016/s0166-2236(98)01327-7).
- Spann, B. M., and I. Grofova. 1991. "Nigropedunculopontine Projection in the Rat: An Anterograde Tracing Study With Phaseolus Vulgaris-Leucoagglutinin (PHA-L)." *Journal of Comparative Neurology* 311, no. 3: 375–388. <https://doi.org/10.1002/cne.903110308>.
- Tovote, P., M. S. Esposito, P. Botta, et al. 2016. "Midbrain Circuits for Defensive Behaviour." *Nature* 534, no. 7606: 206–212. <https://doi.org/10.1038/nature17996>.
- Trachtenberg, J., B. Chen, G. Knott, et al. 2002. "Long-Term in Vivo Imaging of Experience-Dependent Synaptic Plasticity in Adult Cortex." *Nature* 420, no. 6917: 788–794. <https://doi.org/10.1038/nature01273>.
- Tubert, C., D. Galtieri, and D. J. Surmeier. 2019. "The Pedunculopontine Nucleus and Parkinson's Disease." *Neurobiology of Disease* 128: 3–8. <https://doi.org/10.1016/j.nbd.2018.08.017>.
- Villalba, R. M., T. Wichmann, and Y. Smith. 2014. "Neuronal Loss in the Caudal Intralaminar Thalamic Nuclei in a Primate Model of Parkinson's Disease." *Brain Structure and Function* 219, no. 1: 381–394. <https://doi.org/10.1007/s00429-013-0507-9>.
- Wang, D.-S., L. Ju, A. G. Pinguelo, et al. 2024. "Crosstalk Between GABA_A Receptors in Astrocytes and Neurons Triggered by General Anesthetic Drugs." *Translational Research* 267: 39–53. <https://doi.org/10.1016/j.trsl.2023.11.007>.
- Waszczak, B. L. and J. R. Walters. 1984. "A Physiological Role for Dopamine as Modulator of GABA Effects in Substantia Nigra: Supersensitivity in 6-Hydroxydopamine-Lesioned Rats." *European Journal of Pharmacology* 105, no. 3-4: 369–373.

Supporting Information

Additional supporting information can be found online in the Supporting Information section.